Simultaneous extraction of fragmentation functions of light charged hadrons with mass corrections

Maryam Soleymaninia,[1,*] Muhammad Goharipour,[1,†] Hamzeh Khanpour,[2,1,‡] and Hubert Spiesberger[3,§]

[1]*School of Particles and Accelerators, Institute for Research in Fundamental Sciences (IPM), P.O.Box 19395-5531, Tehran, Iran*

[2]*Department of Physics, University of Science and Technology of Mazandaran, P.O.Box 48518-78195, Behshahr, Iran*

[3]*PRISMA$^+$ Cluster of Excellence, Institut für Physik, Johannes-Gutenberg-Universität, Staudinger Weg 7, D-55099 Mainz, Germany*

(Received 13 August 2020; revised 16 December 2020; accepted 16 March 2021; published 30 March 2021)

Achieving the highest possible precision for theoretical predictions at the present and future high-energy lepton and hadron colliders requires a precise determination of fragmentation functions (FFs) of light and heavy charged hadrons from a global QCD analysis with great accuracy. We describe a simultaneous determination of unpolarized FFs of charged pions, charged kaons and protons/antiprotons from single-inclusive hadron production in electron-positron annihilation (SIA) data at next-to-leading order and next-to-next-to-leading order accuracy in perturbative QCD. A new set of FFs, called `SGKS20`, is presented. We include data for identified light charged hadrons ($\pi^{\pm}$, $K^{\pm}$ and $p/\bar{p}$) as well as for unidentified light charged hadrons, $h^{\pm}$ and show that these data have a significant impact on both size and uncertainties of the fragmentation functions. We examine the inclusion of higher-order perturbative QCD corrections and finite-mass effects. We compare the new `SGKS20` FFs with other recent FFs available in the literature and find in general reasonable agreement, but also important differences for some parton species. We show that theoretical predictions obtained from our new FFs are in very good agreement with the analyzed SIA data, especially at small values of z. The `SGKS20` FF sets presented in this work are available via the `LHAPDF` interface.

DOI: 10.1103/PhysRevD.103.054045

I. INTRODUCTION

The two nonperturbative elements in theoretical high energy cross sections of hard scattering processes are the parton distribution functions (PDFs) and the collinear unpolarized fragmentation functions (FFs) [1–12]. The factorization theorem of quantum chromodynamics (QCD) tells us that these are universal and their evolution can be calculated from perturbative QCD. A precise determination of FFs is crucial for studies of the strong interaction in high energy scattering processes. FFs describe how high energy colored partons produced in the hard interactions are turned into the hadrons measured and identified in an experiment. As is the case for PDFs, FFs need to be determined through a QCD analysis of high-energy experimental data due to their nonperturbative nature. Currently, several experimental measurements from different processes are available which can be used for the determination of FFs. Hadron production in single-inclusive e^+e^- annihilation (SIA) provides the main information on FFs, but measurements from semi-inclusive deep inelastic scattering (SIDIS) and from proton-(anti)proton collisions at hadron colliders can also be used to determine well-constrained FFs. SIDIS and proton-proton collisions are particularly important for a complete flavor decomposition of FFs into quark and antiquark components. However, among these high-energy processes, SIA is the cleanest process and the interpretation of it does not require a simultaneous knowledge of PDFs.

There have been several analyses aiming to extract FFs of the lightest charged hadrons $\pi^{\pm}$, $K^{\pm}$ and $p/\bar{p}$ [2–4,13–19]. The most important experimental information for determining the FFs comes from SIA data and most of the recent analyses have considered only these data to determine FFs up to next-to-next-to-leading order (NNLO) in perturbative QCD. For the case of charged pion, kaon and proton/antiproton analyses which include SIDIS and pp data, we refer to Refs. [11,13,14].

*Maryam_Soleymaninia@ipm.ir
†Muhammad.Goharipour@ipm.ir
‡Hamzeh.Khanpour@cern.ch
§spiesber@uni-mainz.de

Published by the American Physical Society under the terms of the Creative Commons Attribution 4.0 International license. Further distribution of this work must maintain attribution to the author(s) and the published article's title, journal citation, and DOI. Funded by SCOAP^3.

The analyses performed so far for extracting $\pi^{\pm}$, $K^{\pm}$, and $p/\bar{p}$ FFs differ in various aspects, such as the experimental data included, the QCD perturbative order, the phenomenological framework, the error calculation procedure, and so on. In particular we note that up to now, it was customary to analyze the light charged hadron data independently from each other, i.e., the extraction of FFs for one type of hadron was solely performed through the analysis of production data for that type of hadron. In contrast, in our most recent study [2], we have shown, for the first time, that a simultaneous analysis of pion and unidentified light charged hadron data for extracting pion FFs is also possible and leads to a reduction in the uncertainties of the extracted pion FFs.

The main goal of the following study, referred to as SGKS20 FFs, is to revisit our previous analysis [2] and extract $\pi^{\pm}$, $K^{\pm}$, and $p/\bar{p}$ FFs simultaneously by including all available SIA data for pion, kaon, proton production along with data for unidentified light charged hadrons $h^{\pm}$. We perform a QCD analysis at next-to-leading order (NLO) as well as at next-to-next-to-leading order (NNLO). Moreover, in the present analysis, we also study hadron mass corrections. We find that these corrections are important at small z, the ratio of momentum transferred from the parton to the observed hadron, and at low values of center-of-mass energy $\sqrt{s}$. Since the contribution of unidentified light charged hadrons $h^{\pm}$ is mostly related to the pion, kaon and proton, we show that the extraction of $\pi^{\pm}$, $K^{\pm}$, and $p/\bar{p}$ FFs in a simultaneous analysis of identified and unidentified light charged hadron production data and including the hadron mass corrections significantly improves the fit quality and leads to well-constrained FFs.

This article is organized in the following manner. In Sec. II we present the SIA data used in our NLO and NNLO FFs analyses, along with their corresponding observables and the kinematic cuts we impose on the data. Then, in Sec. III we discuss the theoretical details of the SGKS20 FFs determination of $\pi^{\pm}$, $K^{\pm}$ and $p/\bar{p}$ FFs, including the parameterizations and the evolution of FFs. Our assumptions and the hadron mass corrections are discussed in this section as well. Section IV deals with the method of χ^2 minimization and estimation of the SGKS20 FFs uncertainties. Considering the best fit parameters, the main results of this study are presented in Sec. V. We first turn to discuss the SGKS20 FFs sets. Then, we compare our best fit obtained for pion, kaon, and proton/antiproton FFs at NNLO with other results in the literature. We also present a detailed comparison between all analyzed SIA data and the corresponding theoretical predictions obtained using the SGKS20 FFs. Finally, in Sec. VI we present our summary and conclusions. We also outline in this section some possible future developments.

II. EXPERIMENTAL OBSERVABLES

The SIA processes have provided us with a wealth of high-precision experimental data carrying information about how partons fragment into a low-mass charged hadron. In this section, we provide details of the experimental measurements used as input for the determination of the SGKS20 FFs along with the corresponding observables and kinematic cuts applied. The simultaneous determination of light charged hadron FFs presented in this work is based on comprehensive datasets from electron-positron annihilation into a single identified and unidentified hadron. In addition to the inclusive measurements, the dataset entering the SGKS20 analysis also includes flavor-tagged measurements.

We note that SIA data are particularly clean, however, they provide only a limited sensitivity to the flavor separation of different light quark FFs. In addition, it is known that the gluon FF is poorly constrained by the total SIA cross section measurements. Hence, in order to improve the discrimination between different quark and antiquark flavors, one would have to include SIDIS and hadron collider observables. This is, however, beyond the scope of the present work.

In our analysis of $\pi^{\pm}$, $K^{\pm}$, $p/\bar{p}$, and $h^{\pm}$ data, we will include all available SIA measurements from different experiments and with different center-of-mass energies. For the case of $\pi^{\pm}$, $K^{\pm}$, and $p/\bar{p}$, we use the data from the BELLE, *BABAR*, TASSO, TPC, TOPAZ, ALEPH, DELPHI, OPAL, and SLD Collaborations [20–32]. These data are based on inclusive cross section measurements which contain all quark flavors, as well as flavor-tagged light (uds)-, charm (c)-, and bottom (b)-quark samples. Note that constraints on heavy quark FFs is provided by the heavy flavor-tagged data.

For the case of unidentified light charged hadron $h^{\pm}$ data, we use the SIA measurements by the TASSO, TPC, ALEPH, DELPHI, OPAL and SLD Collaborations [23,24,27,28,30,31]. The SIA data included in our analysis are listed in Tables I and II. The second column of these tables contains the value of the center-of-mass energy for each experiment. The data cover center-of-mass energies between 10.52 GeV and 91.2 GeV. The total number of data points included is 1492. This combines 392 data points for unidentified light charged hadrons $h^{\pm}$, 412 for pions, 369 for kaons and 319 for protons.

The details of our fitting procedure will be discussed below, but we present already here, in the last four columns of Tables I and II, the values of χ^2 per number of data points, $\chi^2/(N_{\rm pts})$, for each dataset. The value of the total χ^2 per number of degrees of freedom, $\chi^2/(\text{d.o.f.})$, is shown in the last line of these tables. It should be noted that the number of data points of each dataset shown in the tables is subject to kinematic cuts. Actually, we remove data points at small- and large-z in order to avoid regions where resummation effects are sizeable.

We have examined a variety of kinematic cuts for different hadrons at small values of z. Since we include hadron mass effects in our analysis which could affect the

TABLE I. The list of input datasets for $\pi^{\pm}$, $K^{\pm}$, $p/\bar{p}$, and $h^{\pm}$ production included in the present analysis. For each dataset, we have indicated the corresponding reference and the center-of-mass energy $\sqrt{s}$. In the last four columns we show the value of $\chi^2/N_{\rm pts}$ resulting from the FF fit at NLO order. The total value of χ^2/d.o.f. is shown at the bottom of the table.

Experiment	$\sqrt{s}$	$\frac{\chi^2}{N_{\rm pts}}(\pi^{\pm})$	$\frac{\chi^2}{N_{\rm pts}}(K^{\pm})$	$\frac{\chi^2}{N_{\rm pts}}(p/\bar{p})$	$\frac{\chi^2}{N_{\rm pts}}(h^{\pm})$
BELLE [20]	10.52	0.467	0.966	…	…
BABAR [21]	10.54	1.793	2.838	1.017	…
TASSO12 [22]	12	1.154	0.930	0.648	…
TASSO14 [23,32]	14	1.202	1.447	2.237	0.607
TASSO22 [23,32]	22	2.461	2.472	1.969	0.628
TPC [24]	29	0.601	0.664	4.419	0.636
TASSO30 [22]	30	…	…	1.239	…
TASSO34 [25]	34	1.265	0.136	1.704	…
TASSO35 [23]	34	…	…	…	1.165
TASSO44 [23,25]	44	2.052	…	…	0.770
ALEPH [26,27]	91.2	1.876	0.797	2.248	0.814
DELPHI (incl.) [28]	91.2	1.274	0.731	0.559	0.537
DELPHI (*uds* tag) [28]	91.2	0.813	1.062	0.671	0.378
DELPHI (*b* tag) [28]	91.2	0.928	0.632	0.817	0.374
OPAL (incl.) [29,30]	91.2	1.455	0.879	…	0.682
OPAL (*uds* tag) [29,30]	91.2	…	…	…	0.554
OPAL (*c* tag) [29,30]	91.2	…	…	…	0.619
OPAL (*b* tag) [29,30]	91.2	…	…	…	0.232
SLD (incl.) [31]	91.2	1.865	0.578	0.824	0.307
SLD (*uds* tag) [31]	91.2	1.602	2.045	1.690	0.669
SLD (*c* tag) [31]	91.2	0.880	1.087	2.905	0.592
SLD (*b* tag) [31]	91.2	0.702	1.214	2.888	0.170
Total χ^2/d.o.f.			1685.057/1438 = 1.171		

TABLE II. Same as Table. I but for the SGKS20 FFs fit at NNLO.

Experiment	$\sqrt{s}$	$\frac{\chi^2}{N_{\rm pts}}(\pi^{\pm})$	$\frac{\chi^2}{N_{\rm pts}}(K^{\pm})$	$\frac{\chi^2}{N_{\rm pts}}(p/\bar{p})$	$\frac{\chi^2}{N_{\rm pts}}(h^{\pm})$
BELLE [20]	10.52	0.295	0.993	…	…
BABAR [21]	10.54	1.504	2.503	0.234	…
TASSO12 [22]	12	1.135	0.933	0.669	…
TASSO14 [23,32]	14	1.194	1.392	2.166	0.627
TASSO22 [23,32]	22	2.348	2.580	1.920	0.697
TPC [24]	29	1.099	0.519	4.814	0.438
TASSO30 [22]	30	…	…	1.339	…
TASSO34 [25]	34	1.136	0.175	1.496	…
TASSO35 [23]	34	…	…	…	1.362
TASSO44 [23,25]	44	2.129	…	…	0.799
ALEPH [26,27]	91.2	1.362	0.747	0.991	0.738
DELPHI (incl.) [28]	91.2	1.471	0.684	0.541	0.508
DELPHI (*uds* tag) [28]	91.2	0.991	1.050	0.578	0.413
DELPHI (*b* tag) [28]	91.2	0.850	0.651	1.537	0.295
OPAL (incl.) [29,30]	91.2	1.380	1.126	…	0.780
OPAL (*uds* tag) [29,30]	91.2	…	…	…	0.552
OPAL (*c* tag) [29,30]	91.2	…	…	…	0.624
OPAL (*b* tag) [29,30]	91.2	…	…	…	0.175
SLD (incl.) [31]	91.2	1.181	0.549	0.831	0.289
SLD (*uds* tag) [31]	91.2	1.186	2.065	1.197	0.604
SLD (*c* tag) [31]	91.2	0.818	0.992	3.661	0.617
SLD (*b* tag) [31]	91.2	0.667	1.282	2.664	0.140
Total χ^2/d.o.f			1558.169/1438 = 1.083		

small-z region, we include more small-z data points in our QCD fits than has been done in previous studies. Here we provide some details about the choice of the interval $[z_{\min}, z_{\max}]$ in which data points are included in our fit. In general, our choice for $z_{\min}$ and $z_{\max}$ varies with the center-of-mass energy. Choosing the same value of $z_{\min} = 0.02$ for all experiments and for all center-of-mass energies leads to $\chi^2/\text{d.o.f.} = 1.415$ and 1.228 for our NLO and NNLO analyses, respectively. Choosing the values of $z_{\min} = 0.075$ instead of 0.02 leads to $\chi^2/\text{d.o.f.} = 1.167$ and 1.131 for the NLO and NNLO analyses, respectively. We found that it is indeed much better to include the data points with $z \geq 0.02$ for the center-of-mass energy of $\sqrt{s} = M_Z$, and $z \geq 0.075$ for $\sqrt{s} < M_Z$, where M_Z is the mass of Z boson, for all different hadrons considered in the analysis. After imposing these kinematical cuts, we end up with a total of $N_{\text{pts}} = 1492$. As shown in Tables I and II, with these choices of kinematic cuts we find $\chi^2/\text{d.o.f.} = 1.171$ for NLO and $\chi^2/\text{d.o.f.} = 1.083$ for the NNLO fit, i.e., the NNLO fit shows in general a better fit quality.

Compared with the most recent analysis by the `NNFF1.0` collaboration [3], we use the same datasets for the identified light charged hadron production. However, our analysis is enriched with the additional unidentified light charged hadron production datasets. We agree with `NNFF1.0` in the choice of $z_{\min}$: $z_{\min} = 0.02$ for experiments at $\sqrt{s} = M_Z$, and $z_{\min} = 0.075$ for all other experiments. However, `NNFF1.0` use only data up to $z_{\max} = 0.9$ for all experiments.

III. THE QCD FRAMEWORK FOR THE `SGKS20` FFS

In this section, we turn to present our theoretical framework to perform a simultaneous determination of charged pion, charged kaon, and proton/antiproton FFs using the available SIA experimental data, together with data for unidentified light charged hadron production.

It is, of course, impossible to determine a set of functions from a finite set of data points. One has to assume an ansatz which reduces the unknown functional dependence to a finite set of parameters. The particular choice is always a compromise between physical motivation and flexibility, and a certain amount of bias resulting from a too restrictive choice is unavoidable.

In the present analysis, following Ref. [2], we parametrize all the charged pion, charged kaon, and proton/antiproton FFs at the input scale $\mu_0 = 5$ GeV, using the following functional form:

$$D_i^H(z, Q_0) = \frac{\mathcal{N}_i z^{\alpha_i}(1-z)^{\beta_i}[1+\gamma_i(1-z)^{\delta_i}]}{B[2+\alpha_i, \beta_i+1] + \gamma_i B[2+\alpha_i, \beta_i+\delta_i+1]}, \tag{1}$$

where $B[a, b]$ is the Euler Beta function, H refers to the type of hadron, $H = \pi^{\pm}$, $K^{\pm}$ or $p/\bar{p}$, i denotes the parton type, and $\mathcal{N}_i$ is the normalization constant for each flavor which is considered to be a fit parameter.

Data provide information for inclusive and flavor tagged hadron production, i.e., we can expect that there is sufficient information to separate light flavor from charm- and bottom-quark initiated fragmentation. The separation of the gluon and the light-flavor FFs enters indirectly through the scale dependence. In particular, light flavors are separated by the fact that up- and down-quarks enter with scale-dependent coupling weights [3]. We therefore consider FFs for the flavor combinations $i = u^+$, d^+, s^+, c^+, b^+, and the gluon g, where $q^+ = q + \bar{q}$. SIA data allow us to consider only the sum of quark and anti-quark FFs since these data provide information on certain hadron species summed over the two charge states.

For the $\pi^{\pm}$ FFs, we use isospin symmetry and relate

$$D_{u^+}^{\pi^{\pm}} = D_{d^+}^{\pi^{\pm}}.$$

For the proton/antiproton FFs, we parametrize d^+ and s^+ FFs, as described above in Eq. (1), but assume that the u^+ FF has the same shape as the d^+ FF, i.e., these two FFs are related by a z-independent normalization factor $\mathcal{N}$ [8],

$$D_{u^+}^{p/\bar{p}} = \mathcal{N} D_{d^+}^{p/\bar{p}}. \tag{2}$$

For the case of kaon FFs, one cannot assume that u and d FFs are related in the same way as for pions. The d quark to kaon fragmentation is unfavored. We therefore allow all light-flavor kaon FFs to be different,

$$D_{u^+}^{K^{\pm}} \neq D_{d^+}^{K^{\pm}} \neq D_{s^+}^{K^{\pm}}.$$

This parametrization with 6 independent kaon FFs provides us with additional flexibility and follows the choice of other studies [15,33], but differs from the one in Ref. [3] for `NNFF1.0` where only a 5-component parametrization for the kaon FFs was used.

Data with unidentified light charged hadrons contain additional information which can provide further constraints on the determination of FFs. In our recent analysis of pion FFs [2], we could show that the inclusion of data for unidentified light charged hadrons affected the determination of pion FFs and has also led to a reduction of their uncertainties in some kinematic regions. We are therefore motivated to include unidentified hadrons also in the present analysis.

By definition, unidentified light charged hadrons include $\pi^{\pm}$, $K^{\pm}$, $p/\bar{p}$, and an additional small *residual* contribution from other light hadrons. Hence, the FFs of unidentified light charged hadrons is given by

$$D_i^{h^\pm} = D_i^{\pi^\pm} + D_i^{K^\pm} + D_i^{p/\bar{p}} + D_i^{\mathrm{res}^\pm}. \tag{3}$$

The residual light hadrons contribution is expected to be rather small. However, the most recent study in Ref. [34] shows that the contribution from residual hadrons is significant for the case of c- and b-tagged cross sections. We consider a simple parametrization for the residual light hadron FFs $D^{\mathrm{res}^\pm}$ as described in Ref. [34]. It is given by

$$D_i^{\mathrm{res}^\pm}(z, Q_0) = \mathcal{N}_i \frac{z^{\alpha_i}(1-z)^{\beta_i}}{B[2+\alpha_i, \beta_i + 1]}, \tag{4}$$

where i refers to u^+, d^+, s^+, c^+, b^+ and g. The normalization $\mathcal{N}_i$ of the FFs will be determined along with the other free parameters α_i and β_i from the fit to the data. Since the analyzed SIA data are not sensitive to the separation of light quark flavors (u, d, s), we assume an SU(3) flavor symmetric ansatz,

$$D_{u^+}^{\mathrm{res}^\pm} = D_{d^+}^{\mathrm{res}^\pm} = D_{s^+}^{\mathrm{res}^\pm}.$$

With these assumptions we have introduced 12 additional fit parameters for the residual light hadron FFs.

The currently available SIA data do not fully constrain the entire z dependence of quark and gluon FFs presented in Eqs. (1) and (4). Consequently, we are forced to make some further restrictions on the parameter space of the FFs. In particular, we found that the parameters γ and δ are not well constrained by the SIA data. Therefore we consider them equal to zero for each flavor i of the $K^\pm$ and $p/\bar{p}$ FFs, and also for the s^+, c^+, and g FFs of $\pi^\pm$. To be more precise, just the u^+ and b^+ FFs of pions are considered to include five free parameters. In addition we found that the parameters $\alpha_{s^+}^{\pi^\pm}$, $\alpha_{s^+}^{K^\pm}$, $\beta_{c^+}^{p/\bar{p}}$, and $\beta_{b^+}^{p/\bar{p}}$ are not well constrained by SIA data and we have fixed them at their best values which were found in prefits. Finally, for the residual light hadron FFs, the parameters α and β for the u^+, d^+, s^+, c^+ and the gluon FFs and α for the b^+ FF are only loosely determined by the fit and we fix them as well.

We find that these restrictions of the shape parameters of FFs only marginally limit the freedom of the input functional form for the kaon and proton/antiproton FFs. In total, we have 54 free fit parameters which we include in the FFs uncertainty estimation.

Our results show that taking into account these residual contributions decreases the χ^2/d.o.f. from 1.297 to 1.171 for the NLO analysis and from 1.261 to 1.083 for our NNLO analysis which in general indicates a better agreement of data and theory. We observe that the residual FFs obtained from the combined fit of the present work agree very well with the previous determination described in Ref. [34] where the $D_i^{\mathrm{res}^\pm}$ have been found using `NNFF1.0` FFs for the identified hadrons.

As indicated, mass effects in pion, kaon, and proton production are included in our QCD analysis. According to the definition of unidentified light charged hadrons in Eq. (3) and considering the fact that most of the contributions of light hadrons in unidentified light hadrons is relevant to the pion, kaon, and proton, respectively, including their mass corrections is expected to improve the results, especially in the region of small z and small $\sqrt{s}$. Hadron mass effects have been studied in Ref. [11,35] for e^+e^- annihilation processes. We follow the strategy described in these references and incorporate hadron mass effects in single inclusive hadron production in SIA. For zero hadron mass, the scaling variable is expressed as $z = 2E_H/\sqrt{s}$. A finite value of the hadron masses can be incorporated by a specific choice of the scaling variable. We define the light-cone scaling variable η as

$$\eta = \frac{z}{2}\left(1 + \sqrt{1 - \frac{4m_H^2}{sz^2}}\right), \tag{5}$$

where m_H is the hadron mass. Accordingly, the differential cross section in the presence of hadron mass effects reads

$$\frac{d\sigma}{dz} = \frac{1}{1 - \frac{m_H^2}{s\eta^2}} \sum_a \int_\eta^1 \frac{dx_a}{x_a} \frac{d\hat{\sigma}_a}{dx_a} D_a^H\left(\frac{\eta}{x_a}, \mu\right). \tag{6}$$

According to Eqs. (5) and (6), the hadron mass corrections are most relevant in the small-z and low-$\sqrt{s}$ regions. These formulas are applied for all three types of hadrons, i.e., pions, kaons and protons. The values of the hadron masses used in Eqs. (5) and (6) are considered to be $m_\pi = 0.140$ GeV, $m_K = 0.494$ GeV, and $m_p = 0.938$ GeV. We omit the hadron mass corrections for unidentified hadrons.

We note that the effects of accounting for nonzero hadron masses in extracting the light hadron FFs have been explored recently also by `NNFF1.0` for the case of pions, kaons, and protons FFs [3]. It was observed that hadron-mass corrections can become significant in the kinematic region covered by the SIA data. Indeed, our present analysis confirms that hadron-mass corrections do improve the fit quality. Our detailed investigations show that ignoring these corrections in our QCD fits would lead to larger values of χ^2. At NLO we find χ^2/d.o.f. $= 1.280$ and at NNLO χ^2/d.o.f. $= 1.241$ if mass effects are omitted, while with mass effects included the corresponding values decrease to 1.171 and 1.083 for NLO and NNLO, respectively.

In the present study, we use the publicly available `APFEL` package [36] for both evolving FFs and performing the numerical calculation of the SIA cross sections. Note that, using `APFEL`, the related calculations can be performed up to NNLO accuracy in QCD. We should stress here that measurements of the longitudinal SIA cross-section $(d\sigma_L^{h^\pm}/dz)$ are only available for the production of

unidentified hadrons, $h^{\pm}$. However, one cannot analyze these data at NNLO as perturbative corrections to the coefficient functions are only available up the NLO accuracy in this case [1]. Hence, we omit the data from the measurements of the longitudinal SIA cross section. The effect of heavy quark masses are not taken into account in the present analysis and we use the zero mass variable flavor number scheme (ZM-VFNS) with five active flavors, including charm and bottom FFs. Moreover, the value of the strong coupling constant at the scale of the Z boson mass is considered to be $\alpha_s(M_Z^2) = 0.118$ [37]. For performing minimization and determination of fit parameters, we use the CERN program MINUIT [38]. The definition of χ^2 is the same as the one we used in our previous works [2,6], including the overall normalization errors of the experimental datasets. For calculating the uncertainties of the extracted FFs, we use the standard "Hessian" approach [39,40] with $\Delta\chi^2 = 1$ (for further details, see Ref. [6]). We will briefly describe our method of minimization and uncertainty estimation in the next section.

The best values of the fit parameters for charged pion, charged kaon, proton/antiproton, and residual light hadrons FFs determined at the initial scale $\mu_0 = 5$ GeV are listed in Tables III and IV at NLO and NNLO accuracy, respectively.

TABLE III. Best-fit parameters for the fragmentation of partons into $\pi^{\pm}$, $K^{\pm}$, $p/\bar{p}$, and residual light charged hadrons (res$^{\pm}$) obtained through a simultaneous analysis at NLO accuracy within the framework described in Sec. III. The starting scale has been taken to be $\mu_0 = 5$ GeV for all parton species. Parameters marked with an asterisk are fixed input quantities.

Parameter	$\pi^{\pm}$	$K^{\pm}$	$p/\bar{p}$	res$^{\pm}$
$\mathcal{N}_{u^+}$	0.9527	0.2531	0.8039	0.0019
α_{u^+}	−0.7271	−0.8381	1.4098	152.1475*
β_{u^+}	1.6150	1.7252	5.3543	15.0465*
γ_{u^+}	4.4861	0*	0*	0*
δ_{u^+}	3.6961	0*	0*	0*
$\mathcal{N}_{d^+}$	0.9527	0.1551	0.0620	0.0019
α_{d^+}	−0.7271	−0.4391	1.4098	152.1475*
β_{d^+}	1.6150	7.6257	5.3543	15.0465*
γ_{d^+}	4.4861	0*	0*	0*
δ_{d^+}	3.6961	0*	0*	0*
$\mathcal{N}_{s^+}$	0.7098	0.3125	0.0200	0.0019
α_{s^+}	0.0311*	−0.5743*	1.1364	152.1475*
β_{s^+}	9.8675	2.0694	2.0407	15.0465*
$\mathcal{N}_{c^+}$	0.7908	0.2770	0.0198	0.030
α_{c^+}	−0.7437	−0.3101	10.8627	5.6831*
β_{c^+}	5.7138	4.9055	52.8237*	11.7035*
$\mathcal{N}_{b^+}$	0.7499	0.2175	0.0049	0.1082
α_{b^+}	−0.2896	0.2811	3.8762	1.6225*
β_{b^+}	5.2067	12.2417	159.332*	6.5464
γ_{b^+}	9.6277	0*	0*	0*
δ_{b^+}	8.8143	0*	0*	0*
$\mathcal{N}_g$	0.4801	0.1018	0.1910	0.0270
α_g	1.5868	9.5790	2.3699	20.4675*
β_g	29.8298	7.5076	7.6487	13.8349*

TABLE IV. Same as Table. III but at NNLO accuracy.

Parameter	$\pi^{\pm}$	$K^{\pm}$	$p/\bar{p}$	res$^{\pm}$
$\mathcal{N}_{u^+}$	0.9243	0.2409	0.7188	0.0019
α_{u^+}	−0.8411	−0.7248	0.6275	144.9869*
β_{u^+}	1.7556	2.0895	4.8433	16.5308*
γ_{u^+}	3.2186	0*	0*	0*
δ_{u^+}	4.3105	0*	0*	0*
$\mathcal{N}_{d^+}$	0.9243	0.2486	0.0860	0.0019
α_{d^+}	−0.8411	−0.6878	0.6275	144.9869*
β_{d^+}	1.7556	5.6757	4.8433	16.5308*
γ_{d^+}	3.2186	0*	0*	0*
δ_{d^+}	4.3105	0*	0*	0*
$\mathcal{N}_{s^+}$	0.8006	0.2614	0.0162	0.0019
α_{s^+}	−0.1781*	−0.6810*	0.6308	144.9869*
β_{s^+}	8.1331	1.6131	1.8532	16.5308*
$\mathcal{N}_{c^+}$	0.8070	0.2836	0.0369	0.0291
α_{c^+}	−0.8247	−0.4406	3.6331	9.8796*
β_{c^+}	5.6455	4.7087	25.0310*	19.1145*
$\mathcal{N}_{b^+}$	0.7686	0.2279	0.0058	0.1246
α_{b^+}	−0.3955	0.1040	3.3027	0.5507*
β_{b^+}	4.9983	11.4295	166.0012*	5.6387
γ_{b^+}	9.2937	0*	0*	0*
δ_{b^+}	8.7525	0*	0*	0*
$\mathcal{N}_g$	0.4669	0.0884	0.1986	0.0115
α_g	0.7742	12.1509	−0.1871	24.6488*
β_g	24.7398	8.6869	3.7138	11.2409*

Note that the parameters labeled with an asterisk (*) are either fixed input quantities, or have been determined in a pre-fit and are kept fixed in the final fit to determine the other fit parameters and their uncertainty ranges.

IV. χ^2 MINIMIZATION AND UNCERTAINTY ESTIMATION

The best values of the independent fit parameters defined in Eq. (1) need to be determined from SIA data by performing a minimization procedure using an effective χ^2 function. This function quantifies the goodness of fit to the SIA data for a given set of fit parameters, $\{p_i\}$. The simplest method to calculate the total $\chi^2(\{p_i\})$ for a set of independent fit parameters $\{p_i\}$ is given by,

$$\chi^2(\{p_i\}) = \sum_i^{n^{\text{data}}} \frac{(\mathcal{O}_i^{\text{data}} - \mathcal{T}_i^{\text{theory}}(\{p_i\}))^2}{(\sigma_i^{\text{data}})^2}, \tag{7}$$

where $\mathcal{O}_i^{\text{data}}$ refer to the experimental observables, and $\mathcal{T}_i^{\text{theory}}$ indicate the corresponding theoretical values at a given z and μ^2. In this study, the experimental errors, σ_i^{data}, in the above equation are calculated from the statistical and systematical errors added in quadrature. However, the analyses available in the literature [39,41–43] have shown that such a simple $\chi^2(\{p_i\})$ definition needs to be modified to account for correlations in the experimental uncertainties.

In particular, most of the SIA data come with an overall normalization uncertainty which is fully correlated within one data set, but uncorrelated between different datasets. Therefore we split the global $\chi^2_{\text{global}}(\{p_i\})$ into contributions from individual data subsets,

$$\chi^2_{\text{global}}(\{p_i\}) = \sum_{n=1}^{n^{\text{exp}}} \mathcal{W}_n \chi^2_n(\{p_i\}), \tag{8}$$

where n^{exp} is the number of individual experimental data sets and $\mathcal{W}_n$ indicates a weight factor for the nth experiment. Then, $\chi^2_n(\{p_i\})$ defined in Eq. (7) needs to be corrected as

$$\chi^2_n(\{p_i\}) = \left(\frac{1-\mathcal{N}_n}{\Delta\mathcal{N}_n}\right)^2 + \sum_{k=1}^{N_n^{\text{data}}} \left(\frac{(\mathcal{N}_n \mathcal{O}_k^{\text{data}} - \mathcal{T}_k^{\text{theory}}(\{p_i\}))}{\mathcal{N}_n \delta D_k^{\text{data}}}\right)^2, \tag{9}$$

in which i runs over all data points and N_n^{data} corresponds to the number of data points in each dataset. In order to determine the best fit parameters of the SGKS20 light charged hadrons FFs, we minimize the $\chi^2_{\text{global}}(\{p_i\})$ function with respect to the fit parameters $\{p_i\}$ presented in Eq. (1). The normalization factors $\Delta\mathcal{N}_n$ need to be fitted along with the independent fit parameters $(\{p_i\})$ and then can be kept fixed. The default value of the weight factors for each experimental dataset is considered to be equal to 1 [44,45].

In the following, we briefly discuss our method to estimate the uncertainties of the SGKS20 light charged hadrons FFs. Three different approaches are available in the literature to estimate the uncertainty. They are based on Lagrange multipliers or Monte-Carlo sampling, but the most commonly used method is the so-called Hessian approach [39]. Following the notation adopted in Refs. [40,46], our uncertainty estimation is done using the standard Hessian approach. In this method, the uncertainty for a fragmentation function, $\Delta D(z)$, can be obtained from linear error propagation. It is given by

$$[\Delta D(z)]^2 = \Delta\chi^2_{\text{global}} \left[\sum_i^n \left(\frac{\partial D(z,\hat{p})}{\partial p_i}\right)^2 C_{ii} + \sum_{i\neq j}^n \left(\frac{\partial D(z,\hat{p})}{\partial p_i}\frac{\partial D(z,\hat{p})}{\partial p_j}\right) C_{ij}\right], \tag{10}$$

where p_i (with $i = 1, 2, ..., n$) denotes the independent free parameters for each FF, n refers to the total number of optimized parameters, and $\hat{p}_i$ comprises the numerical values of the optimized parameters. $C_{i,j} \equiv H^{-1}_{i,j}$ are the elements of the covariance matrix determined in this analysis at the input scale. In order to estimate the uncertainties of the SGKS20 light charged hadrons FFs, we follow the standard parameter-fitting criterion by considering contours of $T = \Delta\chi^2_{\text{global}} = 1$ defining the 68% (1-σ) confidence level (CL). For minimization and the determination of both fit parameters and elements of the covariance matrix we use the publicly available CERN program MINUIT [38].

V. RESULTS OF THE SGKS20 FF ANALYSIS

The following part of this article describes in greater detail the results of the SGKS20 FFs analysis. We focus on the inclusion of higher-order QCD corrections in our NNLO results. We also compare our best fit pion, kaon, and proton/antiproton FFs with their counterparts from the NNFF1.0 analysis [3].

In Tables III and IV we present the best fit parameters for the fragmentation functions of partons into $\pi^{\pm}$, $K^{\pm}$, $p/\bar{p}$ and the residual FFs at NLO and NNLO accuracy, respectively.

The NNLO charged hadron FFs, $zD_i^{H^{\pm}}(z,Q^2)$, for singlet ($D_{\Sigma}^{H^{\pm}} = \sum_q (D_q^{H^{\pm}} + D_{\bar{q}}^{H^{\pm}})$, $q = u,\ d,\ s$), heavy-quark- and gluon-to-hadron fragmentation obtained from the combined fit are illustrated in Figs. 1–3 together with their 1-σ uncertainty bands for charged pions, charged kaons and protons/antiprotons, respectively. The NNLO results from the most recent determination available in the literature, namely the NNFF1.0 FFs, are also shown for comparison. The results at $Q^2 = 100\ \text{GeV}^2$ reveal the following findings. A noticeable feature of the distributions shown in Fig. 1 is the remarkable agreement between our $zD^{\pi^{\pm}}(z,Q^2)$ FFs for heavy and singlet quarks with the corresponding results from NNFF1.0. Figure 1 shows a small difference for the gluon density, especially at small values of z. A further remarkable aspect of the comparison in this figure is related to the size of the uncertainties. For all cases, the SGKS20 1-σ error bands are smaller than those of the corresponding NNFF1.0 FFs.

Our charged kaon $zD^{K^{\pm}}(z,Q^2)$ FFs at NNLO accuracy are shown in Fig. 2 in comparison with the NNFF1.0 FFs. Concerning the shapes of the kaon FFs, a number of interesting differences between the SGKS20 and NNFF1.0 FFs can be seen. The differences in shape among the two FF sets are more marked than in the case of the charged pion FF. Moderate differences are observed for the central value of the singlet FF at smaller values of z, especially at $z < 0.1$, and for the uncertainty band of the bottom FF below $z < 0.05$. A more noticeable difference in shape is observed for the gluon and charm FFs for which the SGKS20 results are more suppressed and enhanced, respectively, at $z < 0.4$, than the gluon and charm FFs from NNFF1.0.

Let us now discuss the SGKS20 protons and antiprotons $zD^{p/\bar{p}}(z,Q^2)$ FFs. A fair agreement is observed only in the case of the heavy-quark and singlet-quark FFs at large values of z. These FFs are more suppressed at medium to small z values, compared with the corresponding FFs from

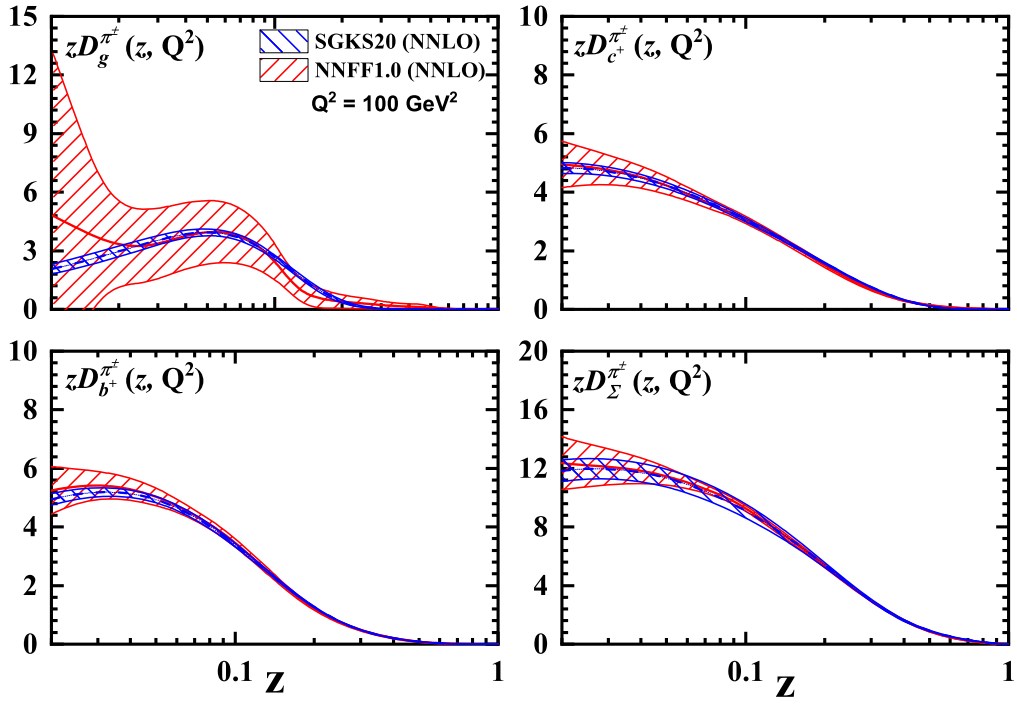

FIG. 1. Comparison of SGKS20 NNLO charged pion FFs, $zD_i^{\pi^\pm}(z, Q^2)$ $(i = g, c, b, \Sigma)$ together with their 1-σ uncertainty bands at $Q^2 = 100$ GeV^2 with the results from the NNFF1.0 Collaboration.

NNFF1.0. For $zD_g^{p/\bar{p}}$, big differences can be seen both in the magnitude and the error band of the FFs in the whole range of z. Overall, the error bands for all heavy quark, singlet and gluon FFs for all light hadrons are dramatically reduced, except for the singlet FF of the kaon at medium to large z.

There are a number of similarities and differences between the SGKS20 and NNFF1.0 analyses. The QCD

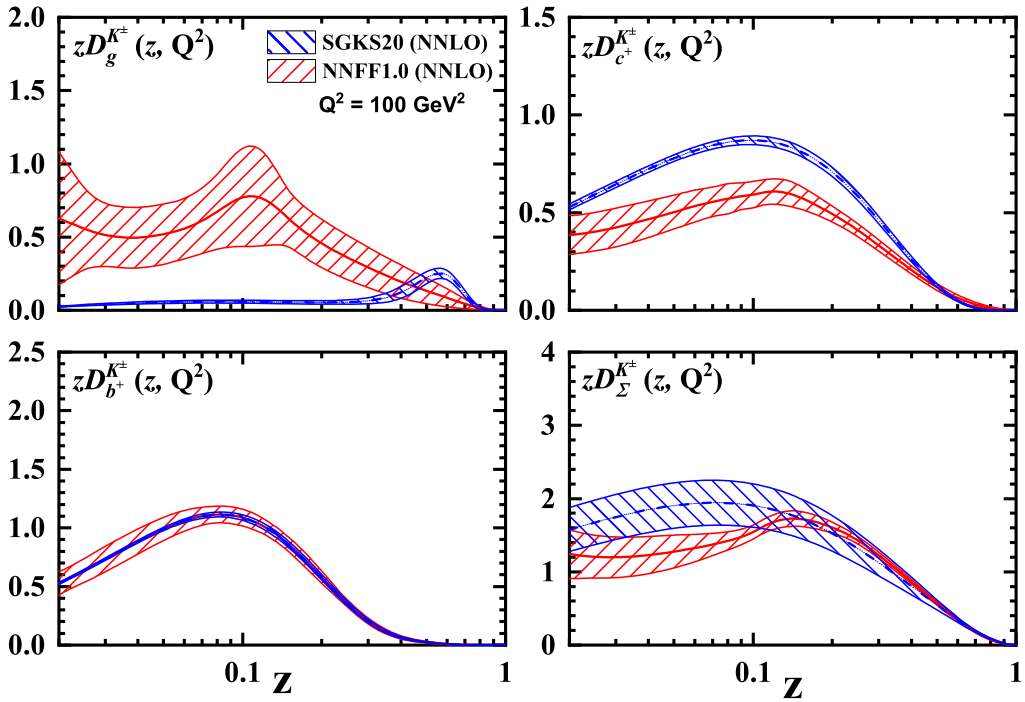

FIG. 2. Same as Fig. 1 but for the charged kaon $zD_i^{K^\pm}(z, Q^2)$ FFs.

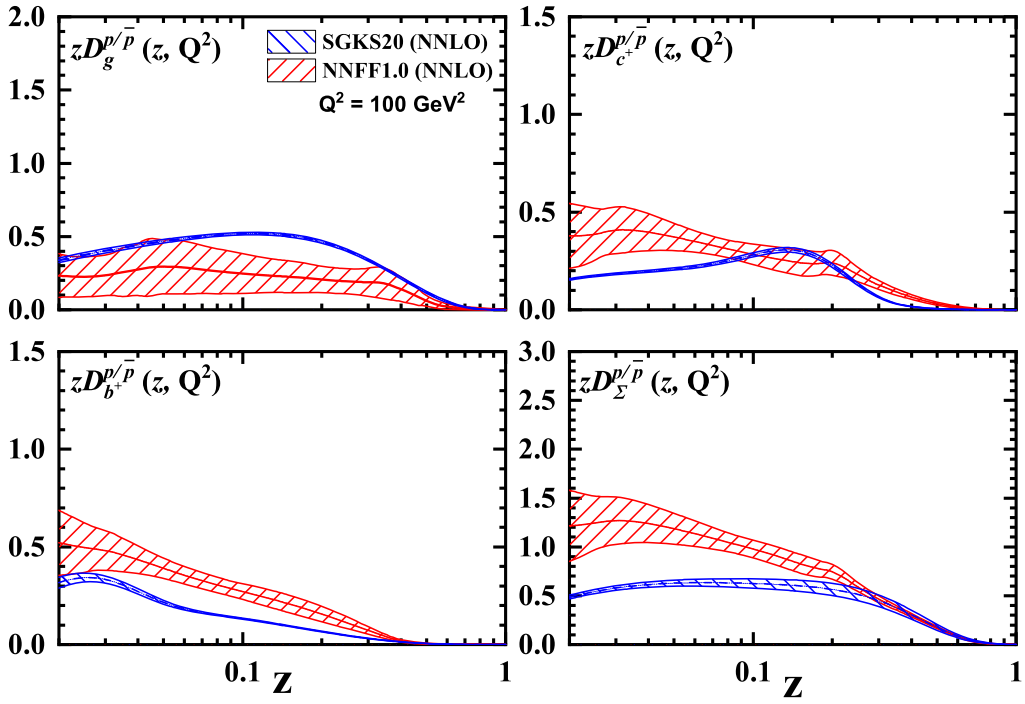

FIG. 3. Same as Fig. 1 but for the proton and antiproton FFs, $zD_i^{p/\bar{p}}(z, Q^2)$.

approach used in this study is similar to the one used by NNFF1.0. In both cases, NNLO QCD and hadron-mass corrections are taken into account. Also, the kinematic cuts imposed on data points in the small z region are the same in both analyses. The origin of the differences between the SGKS20 and NNFF1.0 FFs is likely to be due to the following reasons.

First, the NNFF1.0 approach is based on neural networks without fixing *a priori* a specific parametrization. This allows one to obtain much more flexibility in the

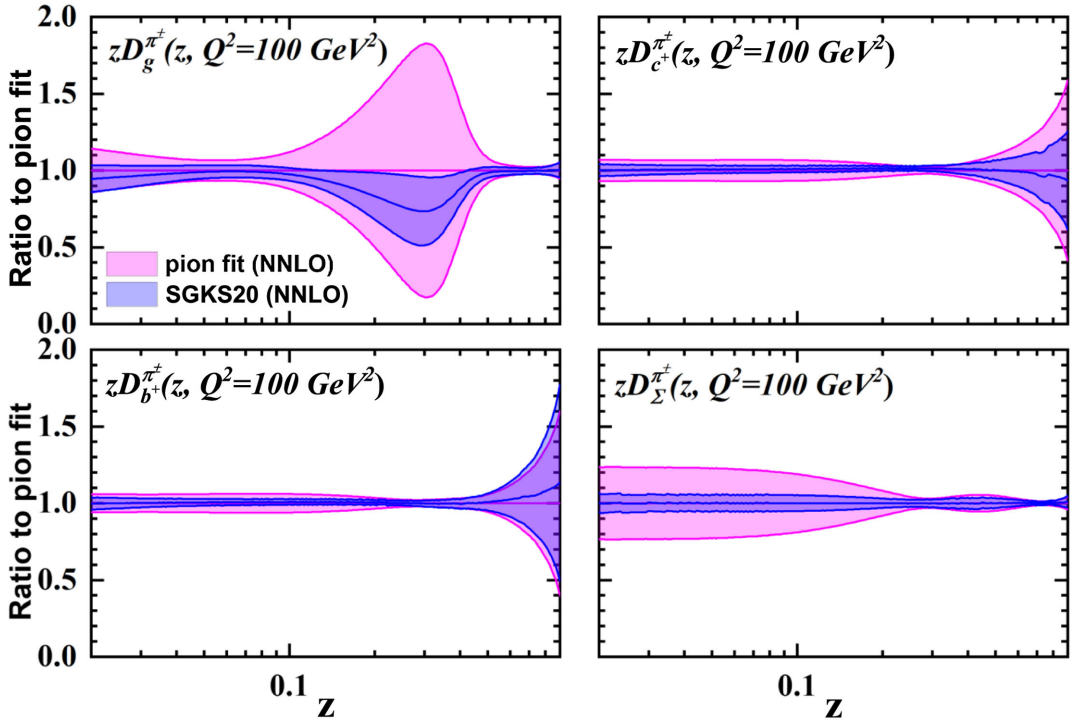

FIG. 4. Comparison of SGKS20 NNLO charged pion FFs, $zD_i^{\pi^\pm}(z, Q^2 = 100\ \mathrm{GeV}^2)$ ($i = g, c, b, \Sigma$) presented in this study with results extracted from a fit without including unidentified light charged hadron data.

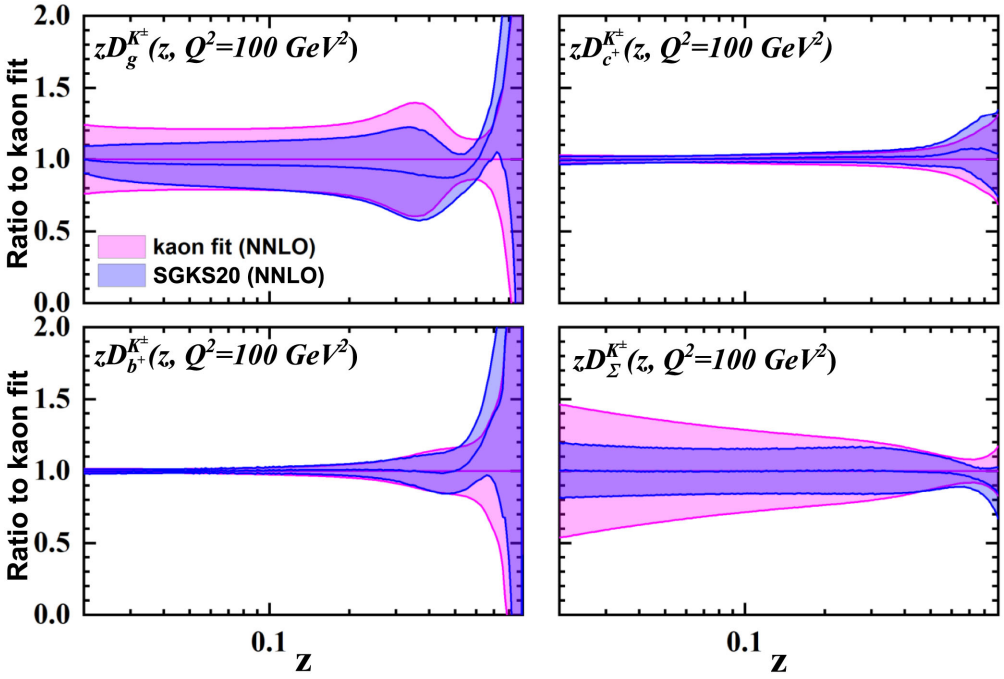

FIG. 5. Same as Fig. 4 but for the charged kaon $zD_i^{K^\pm}(z, Q^2)$ FFs.

description of FFs. In contrast, SGKS20 uses the standard Hessian method with the choice of tolerance $\Delta\chi^2 = 1$ at 68% confidence level. It can, therefore, be expected that the uncertainties of the NNFF1.0 FFs are larger than those of SGKS20. This is indeed the case, as seen in the figures. Second, the origin of differences in the shape and error bands for the SGKS20 FFs is also due to the fact that we include more data in the analysis: data for unidentified light charged hadrons are taken into account along with identified $\pi^\pm$, $K^\pm$ and $p/\bar{p}$ production data, simultaneously in one fit.

In the following, we present a systematic study in order to investigate in more detail the origin of differences between our results and NNFF1.0. We will quantify the

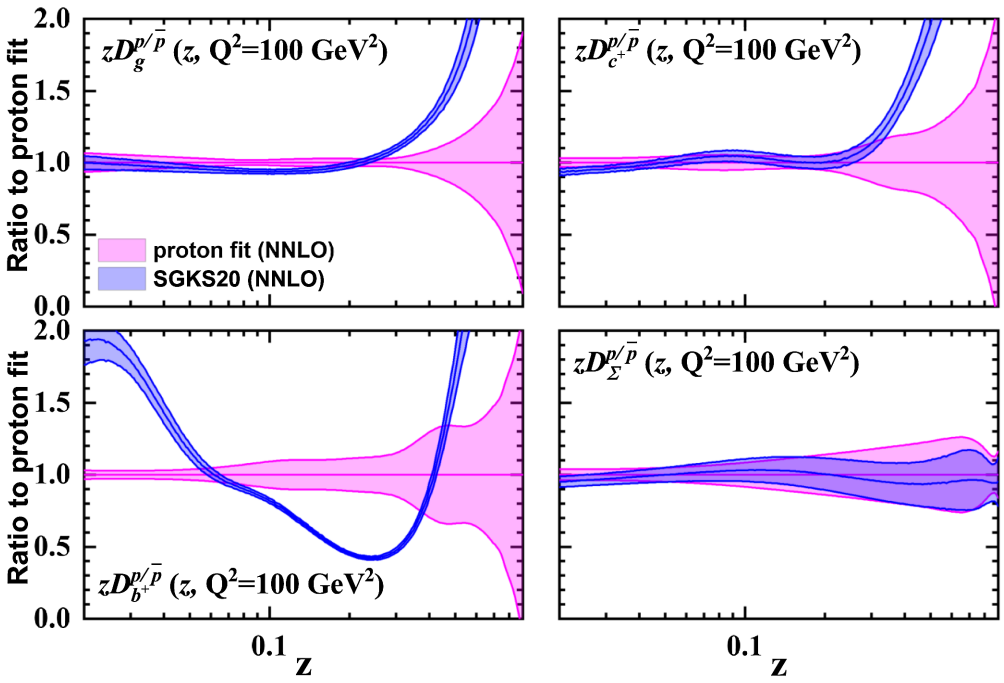

FIG. 6. Same as Fig. 4 but for the proton and antiproton FFs, $zD_i^{p/\bar{p}}(z, Q^2)$.

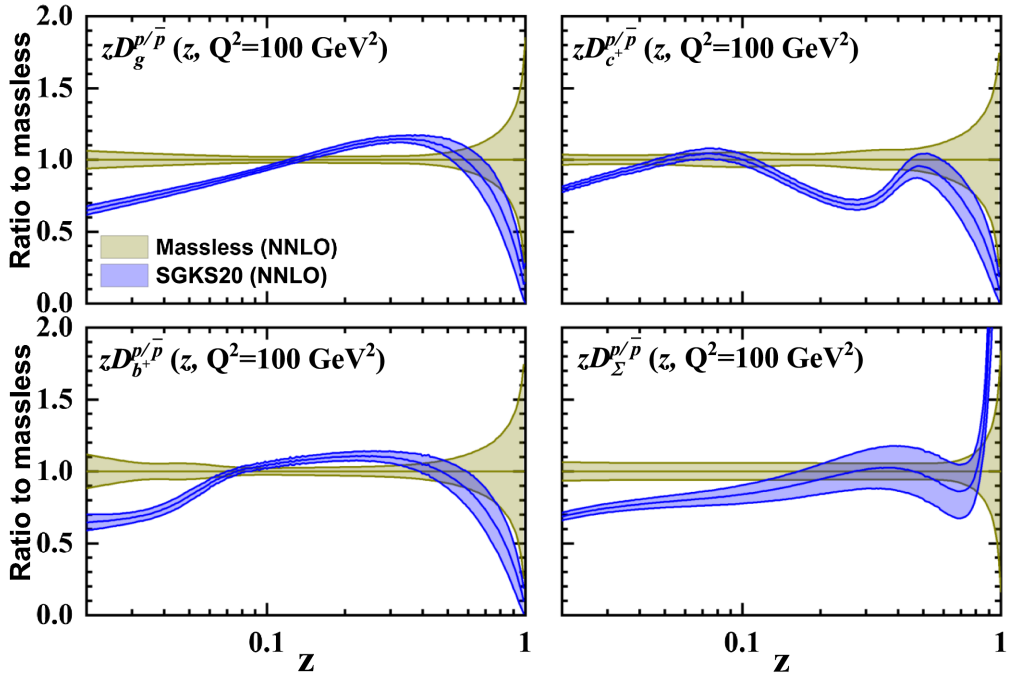

FIG. 7. Comparison of SGKS20 NNLO proton and antiproton FFs presented in this study with results extracted from a QCD analysis without including hadron mass corrections.

additional constraints due to the inclusion of unidentified light charged hadron data. To do so, we have extracted FFs from QCD analyses in which we excluded unidentified light charged hadron data from the fit, i.e., for each of the pion, kaon, and proton FFs we performed separate fits using only data for the respective hadron species. We present the results in terms of ratios where all FFs are normalized to their central values obtained in the separate-hadron fits. In Figs. 4–6 the FFs for $\pi^{\pm}$, $K^{\pm}$, and $p/\bar{p}$ are shown at the reference scale $Q^2 = 100$ GeV^2.

As one can see, the inclusion of unidentified light charged hadron data affect both the shape and the uncertainties of FFs. For all cases, by adding unidentified light charged hadron data, smaller uncertainties are obtained. For the case of pion FFs in Fig. 4, the reduction of the uncertainty bands is clearly visible. The inclusion of unidentified light charged hadron data also affects the shape of the gluon FF of pions. These findings are in good agreement with our previous study [2] where we had examined the effect of such data on the determination of pion FFs.

Similarly, results for the case of charged kaon FFs are presented in Fig. 5. Here again, one can conclude that the inclusion of unidentified light charged hadron data leads to a reduction of the uncertainties in the case of $D_g^{K^{\pm}}$ and $D_{\Sigma}^{K^{\pm}}$, although by a smaller factor than in the case of the pion FFs.

In the case of proton and antiproton FFs, $D_i^{p/\bar{p}}$, we find particularly significant changes of the shape between the "proton fit" and the combined SGKS20 analysis, except for the case of $D_{\Sigma}^{p/\bar{p}}$. The gluon and the heavy-quark FFs are strongly affected at large z, while the b^+ FF changes over the whole range of z. As can be seen in Fig. 6, adding unidentified light charged hadron data also leads to a large reduction of the uncertainty bands, again with the exception of the Σ FF.

Now we also want to discuss in detail the effect arising from the inclusion of hadron mass corrections on the shape and uncertainties of FFs. In Fig. 7, we compare the SGKS20 NNLO proton and antiproton FFs presented in this study with the corresponding results that have been extracted from the QCD analysis in which we exclude hadron mass corrections. Since the mass of the proton is larger than those of the pion and kaon, the effect of hadron mass corrections is expected to be most important for the proton FFs. Hence, we present our results for this case only.

Concerning the shapes of the $p/\bar{p}$ FFs, a number of interesting differences between the two results can be seen from the comparisons in Fig. 7. The inclusion of proton mass corrections affects both the shape and the uncertainty of $p/\bar{p}$ FFs. In particular, the low z region is strongly affected in all cases. There is also a slight reduction of the uncertainties at low z, but this is not particularly strong.

As a short summary, our systematic study has shown that there are significant changes of the FF fit results due to the inclusion of unidentified light charged hadrons. This can explain part of the differences between the SGKS20 and NNFF1.0 fits. A detailed comparison of the results shown in Figs. 1, 2, 3 with those in Figs. 4–6 allows us to conclude that a large part of the differences of the width of the

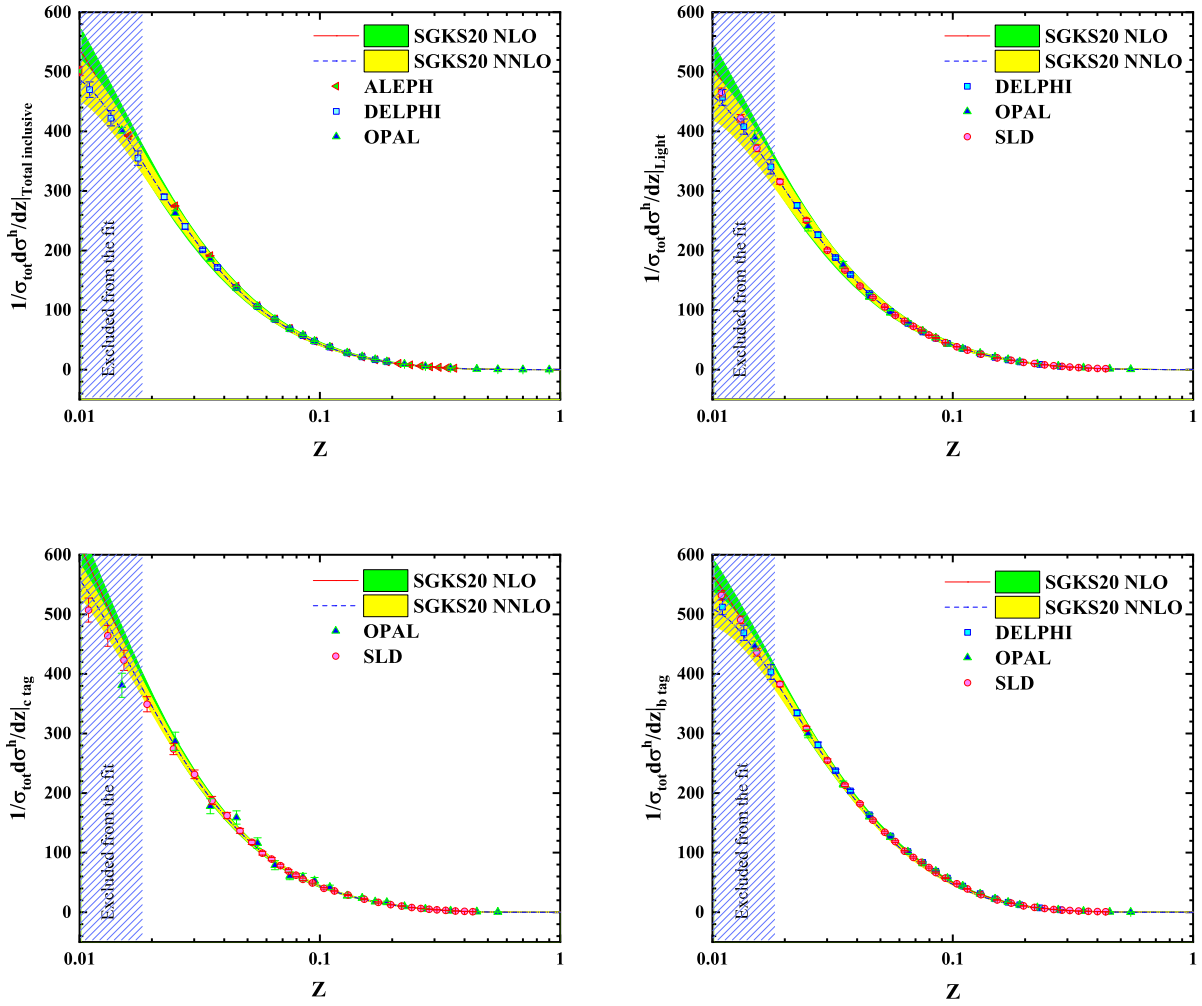

FIG. 8. NLO and NNLO theory predictions for the normalized SIA cross sections of unidentified light charged hadrons in comparison with the total inclusive [26–30], light [28–31], c-tagged [29–31] and b-tagged [28–31] SIA cross section measurements from the ALEPH, DELPHI, OPAL, and SLD experiments. The green (NLO) and yellow (NNLO) shaded bands correspond to uncertainty estimates based on the Hessian approach with $\Delta\chi^2 = 1$.

uncertainty bands is, however, more likely due to the different fit methodology, i.e., due to the fact that we use the Hessian method with a χ^2-based definition of a confidence interval.

Considering the fit quality upon inclusion of higher-order QCD corrections, one can conclude from Tables I and II that the NNLO corrections slightly improve the overall fit quality for almost all SIA data. As one can see from these tables, the $\chi^2/(\text{d.o.f.})$ values at NNLO accuracy are lower than at NLO. Moreover, the fit quality suggests that the inclusion of *residual* light-hadron contributions as well as unidentified light charged hadron data in our identified $zD^{H^\pm}(H^\pm = \pi^\pm, K^\pm, p/\bar{p})$ analysis leads to an improved agreement between theory and data.

Having at hand the SGKS20 NLO and NNLO light charged hadron FFs, we are now able to compare the analyzed data against the theory predictions for the normalized SIA cross sections. In Fig. 8, our theory predictions are compared to the total SIA cross section measurements for inclusive [26–30], light [28–31], c-tagged [29–31] and b-tagged [28–31] unidentified light charged hadron $(h^\pm)$ from ALEPH, DELPHI, OPAL, and SLD experiments. In general, the agreement between data and theory is excellent. In addition, we observe that our NNLO results show a better agreement with the SIA data, especially for the total inclusive, c-tagged and light charged hadron cross sections at small values of z. One can also see that the error bands for the NLO and NNLO theory predictions are very similar, except for the case of c-tagged cross sections where the NNLO predictions show smaller uncertainties.

We also present a comparison of the charged pion, kaon and proton/antiproton data used in this analysis with the corresponding theoretical predictions obtained using our NNLO FFs. In Figs. 9–11, data over theory ratios are displayed for the SLD [31], DELPHI [28] and *BABAR* [21]

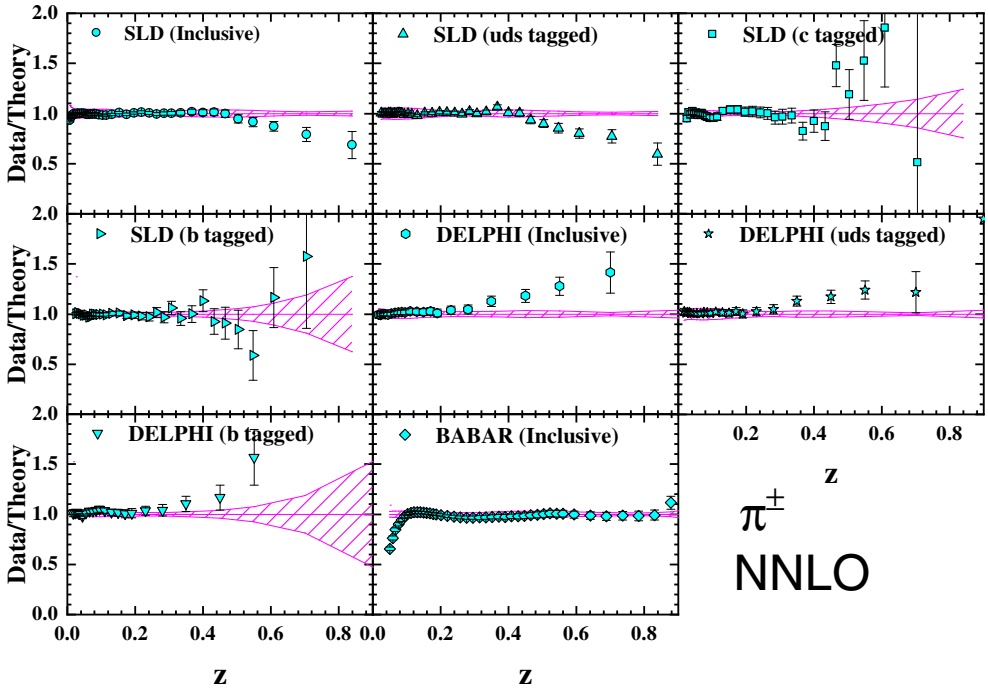

FIG. 9. The data/theory ratio for the charged pion ($\pi^{\pm}$) production data from SLD [31], DELPHI [28], and *BABAR* [21] experiments included in the SGKS20 fit. Our theoretical predictions are computed at NNLO accuracy with our best-fit NNLO FFs.

data for charged pion ($\pi^{\pm}$), charged kaon ($K^{\pm}$), and proton/antiproton ($p/\bar{p}$) production in SIA.

For the case of pion production, Fig. 9, overall good agreement between measurements and the NNLO theory predictions is found for most of the data points, except for the large-z region of some experiments. The uncertainties of our theory predictions are getting large in this region for the case of SLD and DELPHI heavy quark production.

The comparison for charged kaons is presented in Fig. 10. We notice that for some data the agreement is

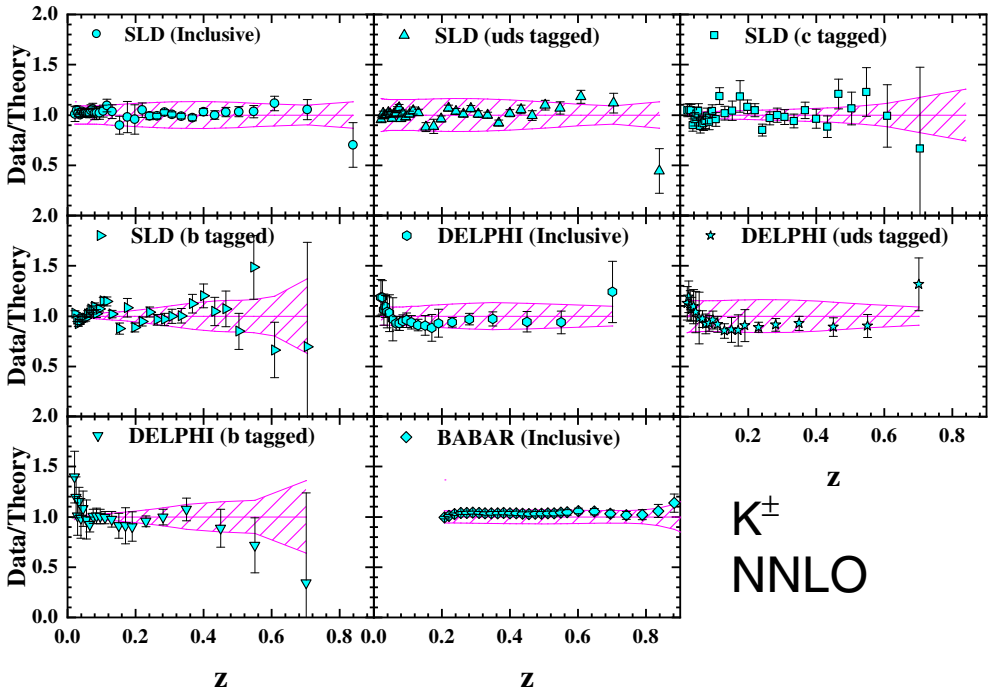

FIG. 10. Same as Fig. 9 but for charged kaons ($K^{\pm}$).

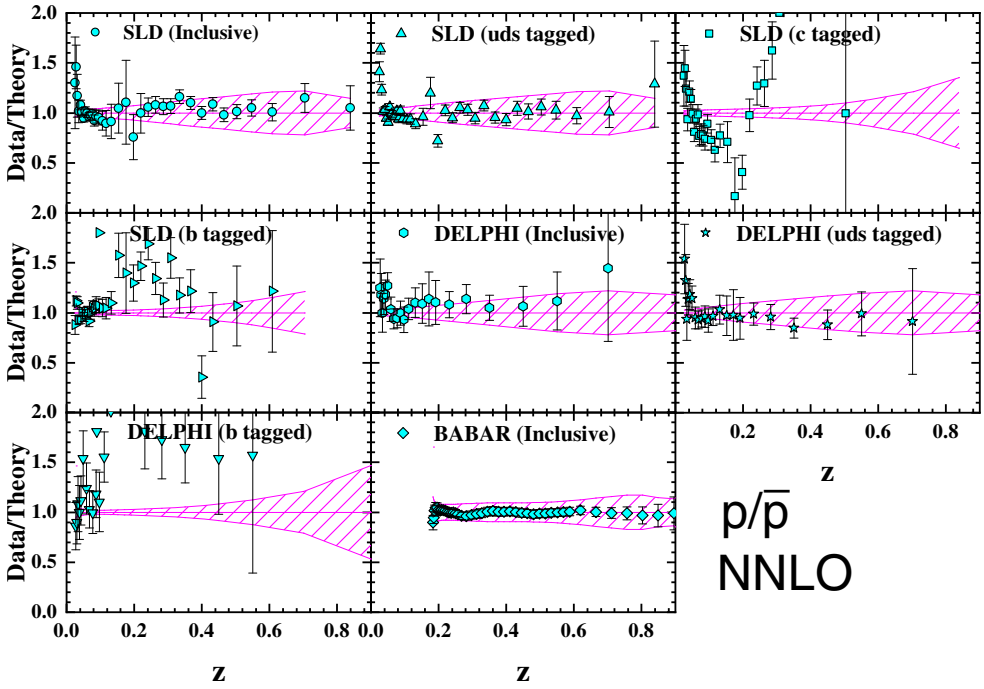

FIG. 11. Same as Fig. 9 but for protons/antiprotons, $(p/\bar{p})$.

good, in particular for the SLD and *BABAR* experiments, while for DELPHI we see some deviations in the small-z region. As one can see, the experimental data points for all datasets fluctuate inside the error bands of the theory predictions.

Finally, we display in Fig. 11 the data/theory ratios for proton/antiproton $(p/\bar{p})$ production for all experimental data analyzed in this work. One can see that for c- and b-tagged data the agreement is poor, but the comparison between our predictions and the total inclusive and uds-tagged data is reasonable. Deviations appear specifically for almost all experiments in the small-z region, except for the case of inclusive measurements from the *BABAR* experiment. For the inclusive measurements of SLD, DELPHI, and *BABAR*, the agreement is acceptable in the medium-to-large range of z-values. The same conclusion can be made for the uds-tagged data from the SLD and DELPHI experiments.

VI. SUMMARY AND CONCLUSIONS

The main goal of the current study is to present a set of FFs, called `SGKS20`, for light charged hadron ($\pi^{\pm}$, $K^{\pm}$, $p/\bar{p}$) production. These FFs are obtained in a simultaneous fit and we include both identified and unidentified light charged hadron data taken from electron-positron annihilation. We included finite-hadron mass corrections which are significant for small z and small $\sqrt{s}$. For FFs which involve heavy quarks, we adopted the zero-mass variable-flavour-number scheme. As a third improvement, the *residual* light hadrons contributions have been included in our fit for unidentified light hadrons. We have shown that this approach improves the total χ^2 at both NLO and NNLO accuracy and also reduces the uncertainties for the FFs of light hadrons. Our results show that the inclusion of higher-order QCD corrections helped to obtain a much better agreement of data with theory. Finally, we compared our pion, kaon and proton FFs with the one recently extracted by the `NNFF1.0` Collaboration.

The most important limitation of the present analysis is related to the fact that we have included data from SIA measurements only. The precise data from proton-(anti) proton (pp) collisions, which cover a wide range in energy and momentum fractions, contain vital information about FFs, especially for the gluon FF, and also are sensitive to different partonic combinations [1]. These measurements include CDF [47,48] experiment at the Tevatron, STAR [49] and PHENIX [50] at RHIC, and CMS [51,52] and ALICE [53] experiments at the LHC. It is expected that the inclusion of these data will lead to much better constrained FFs. Hence, it will be interesting to repeat this analysis by considering the SIDIS data as well as hadron collider data which could provide a flavor separation between quark and antiquark FFs and also the gluon FF. In addition, a future study investigating the improvements of description of the data at low center-of-mass energy due to the effect arising from heavy quarks mass corrections would be very interesting.

The FF parametrizations at NLO and NNLO for identified light charged hadron, $zD^{H^{\pm}}(H^{\pm} = \pi^{\pm}, K^{\pm}, p/\bar{p})$, presented in this study are available in the standard `LHAPDF` format [54] from the authors upon request.

ACKNOWLEDGMENTS

The authors are thankful to Valerio Bertone and Vadim Guzey for many helpful discussions and comments. The authors thank the School of Particles and Accelerators, Institute for Research in Fundamental Sciences (IPM) for financial support of this project. Hamzeh Khanpour also is thankful to the University of Science and Technology of Mazandaran for financial support provided for this research.

[1] V. Bertone, N. P. Hartland, E. R. Nocera, J. Rojo, and L. Rottoli (NNPDF Collaboration), Charged hadron fragmentation functions from collider data, Eur. Phys. J. C **78**, 651 (2018).

[2] M. Soleymaninia, M. Goharipour, and H. Khanpour, Impact of unidentified light charged hadron data on the determination of pion fragmentation functions, Phys. Rev. D **99**, 034024 (2019).

[3] V. Bertone, S. Carrazza, N. P. Hartland, E. R. Nocera, and J. Rojo (NNPDF Collaboration), A determination of the fragmentation functions of pions, kaons, and protons with faithful uncertainties, Eur. Phys. J. C **77**, 516 (2017).

[4] M. Epele, C. García Canal, and R. Sassot, Heavy quark mass effects in parton-to-kaon hadronization probabilities, Phys. Lett. B **790**, 102 (2019).

[5] M. Soleymaninia, H. Khanpour, and S. M. Moosavi Nejad, First determination of D^{*+}-meson fragmentation functions and their uncertainties at next-to-next-to-leading order, Phys. Rev. D **97**, 074014 (2018).

[6] M. Soleymaninia, M. Goharipour, and H. Khanpour, First QCD analysis of charged hadron fragmentation functions and their uncertainties at next-to-next-to-leading order, Phys. Rev. D **98**, 074002 (2018).

[7] M. Soleymaninia, A. N. Khorramian, S. M. Moosavi Nejad, and F. Arbabifar, Determination of pion and kaon fragmentation functions including spin asymmetries data in a global analysis, Phys. Rev. D **88**, 054019 (2013); **89**, A039901 (2014).

[8] D. de Florian, R. Sassot, and M. Stratmann, Global analysis of fragmentation functions for protons and charged hadrons, Phys. Rev. D **76**, 074033 (2007).

[9] G. R. Boroun, S. Zarrin, and S. Dadfar, Laplace method for the evolution of the fragmentation function of B_c mesons, Nucl. Phys. **A953**, 21 (2016).

[10] J. J. Ethier, N. Sato, and W. Melnitchouk, First Simultaneous Extraction of Spin-Dependent Parton Distributions and Fragmentation Functions from a Global QCD Analysis, Phys. Rev. Lett. **119**, 132001 (2017).

[11] S. Albino, B. A. Kniehl, and G. Kramer, AKK update: Improvements from new theoretical input and experimental data, Nucl. Phys. **B803**, 42 (2008).

[12] D. de Florian, R. Sassot, and M. Stratmann, Global analysis of fragmentation functions for pions and kaons and their uncertainties, Phys. Rev. D **75**, 114010 (2007).

[13] D. de Florian, R. Sassot, M. Epele, R. J. Hernández-Pinto, and M. Stratmann, Parton-to-pion fragmentation reloaded, Phys. Rev. D **91**, 014035 (2015).

[14] D. de Florian, M. Epele, R. J. Hernández-Pinto, R. Sassot, and M. Stratmann, Parton-to-kaon fragmentation revisited, Phys. Rev. D **95**, 094019 (2017).

[15] N. Sato, J. J. Ethier, W. Melnitchouk, M. Hirai, S. Kumano, and A. Accardi, First Monte Carlo analysis of fragmentation functions from single-inclusive e^+e^- annihilation, Phys. Rev. D **94**, 114004 (2016).

[16] D. P. Anderle, F. Ringer, and M. Stratmann, Fragmentation functions at next-to-next-to-leading order accuracy, Phys. Rev. D **92**, 114017 (2015).

[17] D. P. Anderle, T. Kaufmann, M. Stratmann, and F. Ringer, Fragmentation functions beyond fixed order accuracy, Phys. Rev. D **95**, 054003 (2017).

[18] S. Albino, B. A. Kniehl, G. Kramer, and C. Sandoval, Confronting fragmentation function universality with single hadron inclusive production at HERA and e+ e- colliders, Phys. Rev. D **75**, 034018 (2007).

[19] B. A. Kniehl, G. Kramer, and B. Potter, Fragmentation functions for pions, kaons, and protons at next-to-leading order, Nucl. Phys. **B582**, 514 (2000).

[20] M. Leitgab *et al.* (Belle Collaboration), Precision Measurement of Charged Pion and Kaon Differential Cross Sections in e^+e^- Annihilation at $\sqrt{s} = 10.52$ GeV, Phys. Rev. Lett. **111**, 062002 (2013).

[21] J. P. Lees *et al.* (*BABAR* Collaboration), Production of charged pions, kaons, and protons in e^+e^- annihilations into hadrons at $\sqrt{s} = 10.54$ GeV, Phys. Rev. D **88**, 032011 (2013).

[22] R. Brandelik *et al.* (TASSO Collaboration), Charged pion, kaon, proton and anti-proton production in high-energy e^+e^- annihilation, Phys. Lett. **94B**, 444 (1980).

[23] W. Braunschweig *et al.* (TASSO Collaboration), Global jet properties at 14 GeV to 44 GeV center-of-mass energy in e^+e^- annihilation, Z. Phys. C **47**, 187 (1990).

[24] H. Aihara *et al.* (TPC/Two Gamma Collaboration), Charged Hadron Inclusive Cross-Sections and Fractions in e^+e^- Annihiliation at $\sqrt{s} = 29$ GeV, Phys. Rev. Lett. **61**, 1263 (1988).

[25] W. Braunschweig *et al.* (TASSO Collaboration), Pion, kaon and proton cross-sections in e^+e^- annihilation at 34 GeV and 44 GeV center-of-mass energy, Z. Phys. C **42**, 189 (1989).

[26] D. Buskulic *et al.* (ALEPH Collaboration), Inclusive $\pi^{\pm}$, $K^{\pm}$ and $(p, \bar{p})$ differential cross-sections at the Z resonance, Z. Phys. C **66**, 355 (1995).

[27] D. Buskulic *et al.* (ALEPH Collaboration), Measurement of alpha-s from scaling violations in fragmentation functions in e^+e^- annihilation, Phys. Lett. B **357**, 487 (1995); Erratum, Phys. Lett. B **364**, 247 (1995).

[28] P. Abreu *et al.* (DELPHI Collaboration), $\pi^{\pm}$, $K^{\pm}$, p and $\bar{p}$ production in $Z^0 \to q\bar{q}$, $Z^0 \to b\bar{b}$, $Z^0 \to u\bar{u}$, $d\bar{d}$, $s\bar{s}$, Eur. Phys. J. C **5**, 585 (1998).

[29] R. Akers *et al.* (OPAL Collaboration), Measurement of the production rates of charged hadrons in e^+e^- annihilation at the Z0, Z. Phys. C **63**, 181 (1994).

[30] K. Ackerstaff *et al.* (OPAL Collaboration), Measurements of flavor dependent fragmentation functions in $Z^0 \to q\bar{q}$ events, Eur. Phys. J. C **7**, 369 (1999).

[31] K. Abe *et al.* (SLD Collaboration), Production of π^+, π^-, K^+, K^-, p and $\bar{p}$ in light (uds), c and b jets from Z^0 decays, Phys. Rev. D **69**, 072003 (2004).

[32] M. Althoff *et al.* (TASSO Collaboration), Charged hadron composition of the final state in e^+e^- annihilation at high-energies, Z. Phys. C **17**, 5 (1983).

[33] M. Hirai, S. Kumano, T. H. Nagai, and K. Sudoh, Determination of fragmentation functions and their uncertainties, Phys. Rev. D **75**, 094009 (2007).

[34] A. Mohamaditabar, F. Taghavi-Shahri, H. Khanpour, and M. Soleymaninia, Determination of contributions from residual light charged hadrons to inclusive charged hadrons from e^+e^- annihilation data, Eur. Phys. J. A **55**, 185 (2019).

[35] S. M. Moosavi Nejad, M. Soleymaninia, and A. Maktoubian, Proton fragmentation functions considering finite-mass corrections, Eur. Phys. J. A **52**, 316 (2016).

[36] V. Bertone, S. Carrazza, and J. Rojo, APFEL: A PDF evolution library with QED corrections, Comput. Phys. Commun. **185**, 1647 (2014).

[37] M. Tanabashi *et al.* (Particle Data Group), Review of particle physics, Phys. Rev. D **98**, 030001 (2018).

[38] F. James and M. Roos, Minuit: A system for function minimization and analysis of the parameter errors and correlations, Comput. Phys. Commun. **10**, 343 (1975); F. James, MINUIT function minimization and error analysis: Reference manual version 94.1, Report No. CERN-D-506, CERN-D506.

[39] A. D. Martin, W. J. Stirling, R. S. Thorne, and G. Watt, Parton distributions for the LHC, Eur. Phys. J. C **63**, 189 (2009).

[40] J. Pumplin, D. Stump, R. Brock, D. Casey, J. Huston, J. Kalk, H. L. Lai, and W. K. Tung, Uncertainties of predictions from parton distribution functions. 2. The Hessian method, Phys. Rev. D **65**, 014013 (2001).

[41] K. Kovarik, I. Schienbein, F. I. Olness, J. Y. Yu, C. Keppel, J. G. Morfin, J. F. Owens, and T. Stavreva, Nuclear Corrections in Neutrino-Nucleus DIS and Their Compatibility with Global NPDF Analyses, Phys. Rev. Lett. **106**, 122301 (2011).

[42] K. Kovarik *et al.*, nCTEQ15—Global analysis of nuclear parton distributions with uncertainties in the CTEQ framework, Phys. Rev. D **93**, 085037 (2016).

[43] I. Schienbein, J. Y. Yu, K. Kovarik, C. Keppel, J. G. Morfin, F. Olness, and J. F. Owens, PDF nuclear corrections for charged and neutral current processes, Phys. Rev. D **80**, 094004 (2009).

[44] D. Stump, J. Pumplin, R. Brock, D. Casey, J. Huston, J. Kalk, H. L. Lai, and W. K. Tung, Uncertainties of predictions from parton distribution functions. 1. The Lagrange multiplier method, Phys. Rev. D **65**, 014012 (2001).

[45] J. Blumlein, H. Bottcher, and A. Guffanti, Non-singlet QCD analysis of deep inelastic world data at O(alpha(s)**3), Nucl. Phys. **B774**, 182 (2007).

[46] J. Pumplin, D. R. Stump, and W. K. Tung, Multivariate fitting and the error matrix in global analysis of data, Phys. Rev. D **65**, 014011 (2001).

[47] F. Abe *et al.* (CDF Collaboration), Transverse Momentum Distributions of Charged Particles Produced in $\bar{p}p$ Interactions at $\sqrt{s} = 630$ GeV and 1800 GeV, Phys. Rev. Lett. **61**, 1819 (1988).

[48] T. Aaltonen *et al.* (CDF Collaboration), Measurement of particle production and inclusive differential cross sections in $p\bar{p}$ collisions at $\sqrt{s} = 1.96$-TeV, Phys. Rev. D **79**, 112005 (2009); , Erratum, Phys. Rev. D **82**, 119903 (2010).

[49] L. Adamczyk *et al.* (STAR Collaboration), Neutral pion cross section and spin asymmetries at intermediate pseudorapidity in polarized proton collisions at $\sqrt{s} = 200$ GeV, Phys. Rev. D **89**, 012001 (2014).

[50] A. Adare *et al.* (PHENIX Collaboration), Inclusive cross-section and double helicity asymmetry for π^0 production in $p + p$ collisions at $\sqrt{s} = 200$ GeV: Implications for the polarized gluon distribution in the proton, Phys. Rev. D **76**, 051106 (2007).

[51] S. Chatrchyan *et al.* (CMS Collaboration), Charged particle transverse momentum spectra in pp collisions at $\sqrt{s} = 0.9$ and 7 TeV, J. High Energy Phys. 08 (2011) 086.

[52] S. Chatrchyan *et al.* (CMS Collaboration), Study of high-pT charged particle suppression in PbPb compared to pp collisions at $\sqrt{s_{NN}} = 2.76$ TeV, Eur. Phys. J. C **72**, 1945 (2012).

[53] B. B. Abelev *et al.* (ALICE Collaboration), Energy dependence of the transverse momentum distributions of charged particles in pp collisions measured by ALICE, Eur. Phys. J. C **73**, 2662 (2013).

[54] A. Buckley, J. Ferrando, S. Lloyd, K. Nordström, B. Page, M. Rüfenacht, M. Schönherr, and G. Watt, LHAPDF6: Parton density access in the LHC precision era, Eur. Phys. J. C **75**, 132 (2015).